# BUTTERWORTH-HEINEMANN SERIES IN CHEMICAL ENGINEERING



**SERIES TITLES**

Bubble Wake Dynamics in Liquids and Liquid-Solid Suspensions
*Liang-Shih Fan* and *Katsumi Tsuchiya*
Chemical Process Equipment: Selection and Design *Stanley M. Walas*
Chemical Process Structures and Information Flows *Richard S.H. Mah*
Computational Methods for Process Simulations *W. Fred Ramirez*
Constitutive Equations for Polymer Melts and Solutions *Ronald G. Larson*
Fluidization Engineering, Second Edition *Daizo Kunii* and *Octave Levenspiel*
Fundamental Process Control *David M. Prett* and *Carlos E. Garcia*
Gas-Liquid-Solid Fluidization Engineering *Liang-Shih Fan*
Gas Separation by Adsorption Processes *Ralph T. Yang*
Granular Filtration of Aerosols and Hydrosols *Chi Tien*
Heterogeneous Reactor Design *Hong H. Lee*
Interfacial Transport Processes and Rheology *David A. Edwards, Howard Brenner,* and *Darsh T. Wasan*
Introductory Systems Analysis for Process Engineers *E. Bruce Nauman*
Microhydrodynamics: Principles and Selected Applications
*Sangtae Kim* and *Seppo J. Karrila*
Modelling with Differential Equations *Stanley M. Walas*
Molecular Thermodynamics of Nonideal Fluids *Lloyd L. Lee*
Phase Equilibria in Chemical Engineering *Stanley M. Walas*
Physicochemical Hydrodynamics: An Introduction *Ronald F. Probstein*
Slurry Flow: Principles and Practice *Clifton A. Shook* and *Michael C. Roco*
Transport Processes in Chemically Reacting Flow Systems *Daniel E. Rosner*
Viscous FLows: The Practical Use of Theory *Stuart W. Churchill*

**REPRINT TITLES**

Advanced Process Control *W. Harmon Ray*
Applied Statistical Mechanics *Thomas M. Reed* and *Keith E. Gubbins*
Elementary Chemical Reactor Analysis *Rutherford Aris*
Kinetics of Chemical Processes *Michel Boudart*
Reaction Kinetics for Chemical Engineers *Stanley M. Walas*

# SLURRY FLOW

## Principles and Practice

**C.A. Shook**
University of Saskatchewan

**M.C. Roco**
University of Kentucky and
National Science Foundation

**Butterworth–Heinemann**
Boston London Oxford Singapore Sydney Toronto Wellington

We dedicate this book to our wives:
Kate Shook and Cathy Roco



**Library of Congress Cataloging-in-Publication Data**

Shook, C.A.
Slurry flow: principles and practice / C.A. Shook, M.C. Roco.
p. cm. — (Butterworth-Heinemann series in chemical engineering)
Includes bibliographical references and index.
ISBN 0–7506–9110–7 (alk. paper)
1. Hydraulic conveying. 2. Slurry. 3. Two-phase flow.
I. Roco, M.C. II. Title. III. Series
TJ898.S53 1991
621.8′67—dc20 91–7514
CIP

**British Library Cataloguing in Publication Data**

Shook, C.A. (Clifton A.)
Slurry Flow: Principles and practice.
1. Slurry. Flow.
I. Title II. Roco, M.C. (M.C.)
532.51

ISBN 0–7506–9110–7

Butterworth–Heinemann
80 Montvale Avenue
Stoneham, MA 02180

10 9 8 7 6 5 4 3 2 1

Printed in the United States of America

We dedicate this book to our wives:
Kate Shook and Cathy Roco



**Library of Congress Cataloging-in-Publication Data**

Shook, C.A.
Slurry flow: principles and practice / C.A. Shook, M.C. Roco.
p. cm. — (Butterworth-Heinemann series in chemical engineering)
Includes bibliographical references and index.
ISBN 0–7506–9110–7 (alk. paper)
1. Hydraulic conveying. 2. Slurry. 3. Two-phase flow.
I. Roco, M.C. II. Title. III. Series
TJ898.S53 1991
621.8′67—dc20 91–7514
CIP

**British Library Cataloguing in Publication Data**

Shook, C.A. (Clifton A.)
Slurry Flow: Principles and practice.
1. Slurry. Flow.
I. Title II. Roco, M.C. (M.C.)
532.51

ISBN 0–7506–9110–7

Butterworth–Heinemann
80 Montvale Avenue
Stoneham, MA 02180

10 9 8 7 6 5 4 3 2 1

Printed in the United States of America

# Preface

This book has been written for the designer and the plant engineer. Our purpose has been to summarize the current state of knowledge in areas of interest to those designing and operating slurry pipelines. In so doing we have assumed a background in fluid mechanics and mathematics, which would be provided by introductory undergraduate courses.

The range of topics is extensive, reflecting the variety of problems associated with slurry flows. In selecting these topics we have drawn upon our experience in testing industrial slurries for purposes of plant design, and in teaching short courses to plant engineers and designers. We realize that many readers, interested in selecting equipment, will turn directly to Chapters 4 to 6 and 8 to 11. Since some of the concepts of fluid, particle, and slurry behavior may be unfamiliar, we hope that Chapters 1 to 3 will provide useful clarifications or direct the reader to the appropriate literature. No description of slurry rheology is complete without an introduction to the role played by surface phenomena and we have tried to do this for readers with a limited background knowledge of chemistry.

There can be little doubt that as research proceeds, mechanistic flow models will provide the framework for generalizing experimental measurements and we have tried to discuss the basis for these models. The modeling task remains as a challenge to the researcher, however, and Chapter 7 indicates the scope of this task.

We have tried to make the book a self-contained source of information for the engineer with a limited technical library. Since our treatment of many concepts must be cursory, we have tried to indicate the literature to which one can turn for further amplification and discussion. The bibliography includes references whose stature would justify their inclusion in a small technical library.

# Chapter 1

# Basic Concepts for Single-Phase Fluids and Particles

## 1.1 STEADY PIPE FLOW

The basic physical principles which govern all flows are conservation of mass, conservation of momentum, and conservation of energy.

In dealing with these physical laws, we choose either a microscopic or a macroscopic control volume. A microscopic control volume is shown in Appendix 1 and the appropriate equations are given there. A macroscopic control volume, which contains the familiar items of equipment found in fluid transport systems, is illustrated in Figure 1–1. The equations expressing the physical laws for a macroscopic control volume are simpler as long as the flow is steady and one dimensional, i.e., one velocity component is of dominant importance.

For steady flow, the mass conservation relationship is

$$\text{Mass flow rate } w = (\text{density } \rho \times \text{velocity } V \times \text{area } A) = \text{constant} \tag{1–1}$$

In terms of the mean values of these quantities at the inlet (1) and outlet (2) of the control volume this means

$$(\rho AV)_1 = (\rho AV)_2$$

The averaging process, by which these mean values are related to the point or local values for incompressible fluid–particle mixtures, is discussed in Appendix 2.

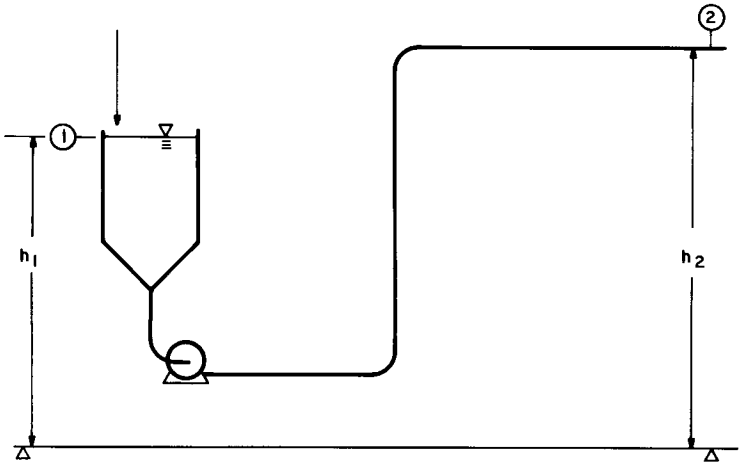


Figure 1–1. A macroscopic control volume.

In a single-phase system the averaging is simpler than it is in a slurry because the density of a single-phase fluid is constant over the cross section. However, the velocity varies with position so that the mean or bulk velocity $V$ is computed by integration of the local velocity $v_x$ in the mean flow ($x$) direction:

$$V = \left(\frac{1}{A}\right)\int_A v_x \, dA = \left(\frac{2\pi}{A}\right)\int_0^{D/2} r v_x \, dr = \frac{Q}{A} \tag{1–2}$$

Equation 1–2 shows that $V$ is the volumetric flow rate per unit area. $\rho AV$ is the mass flow rate that is used in material balance calculations.

The linear momentum equation for the quantities averaged over a pipe cross section may be derived from the differential linear momentum equation for the $x$-direction, Equation A1–6 in Appendix 1, by integrating over the cross section of the pipe (e.g., Longwell, 1966) to give

$$\rho\left[\frac{\partial V}{\partial t} + V\frac{\partial V}{\partial x} + g\frac{\partial h}{\partial x}\right] + \frac{\partial P}{\partial x} + 4\frac{\tau_w}{D} = 0 \tag{1–3}$$

where $t$ denotes time, $P$ is the average pressure, and $\tau_w$ is the resisting wall shear stress. The sign convention for surfaces and stresses is given in Appendix 1. A positive surface of a control volume is defined as one whose normal, in a positive coordinate direction, points *into* the volume. A positive stress acts in a positive coordinate direction on a positive surface or in a negative coordinate direction on a negative surface.

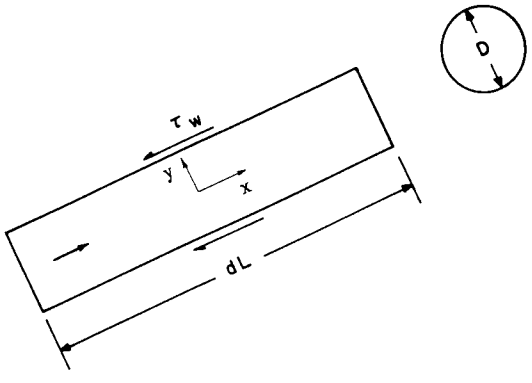


**Figure 1–2.** An elemental control volume for a pipeline.

The extended form of Bernouilli's equation is obtained by integrating the steady flow form of Equation 1–3 in the axial ($x$) direction for the macroscopic control volume. The most useful form of the resultant energy equation is given in Equation 1–4 for a simple pipeline consisting of sections of length $L_i$ and diameter $D_i$. A differential fluid element is shown in Figure 1–2. The curved surface of the element is a negative surface.

$$\int_1^2 \frac{dP}{\rho} + \left[\left(\frac{V^2}{2\alpha}\right)_2 - \left(\frac{V^2}{2\alpha}\right)_1\right] + g(h_2 - h_1) - gH + \sum \frac{4\tau_w L}{\rho D} = 0 \quad (1\text{–}4)$$

The terms in this equation are all expressed in J/kg of fluid. They represent, from left to right, pressure change, kinetic energy change, potential energy change, pump energy input, and frictional dissipation effects. $H$ is the "head" generated by the pump ($H$ is negative for a turbine) and $\tau_w$ is the shear stress that opposes flow at the wall of each pipe section.

$\alpha$ is a correction factor that allows for the fact that all the fluid particles passing through a plane in a given time do not have the same kinetic energy per unit mass. Its value depends on the distribution of the axial velocity $v_x(r)$, where $r$ is the radial coordinate. $\alpha$ ranges between 0.5 (parabolic distribution) and 1.0 (flat).

The wall shear stress $\tau_w$ opposes fluid motion and its sense is therefore opposite to that of $V$. $\tau_w$ is expressed in terms of the Fanning friction factor $f$ as

$$\tau_w = 0.5 f V|V|\rho \quad (1\text{–}5)$$

The absolute value restriction in Equation 1–5 is usually ignored, except in pipe network calculations when the direction of flow is unknown. For Newtonian

fluids (defined in Appendix 1), $f$ can be calculated from the Reynolds number $\mathrm{Re} = D|V|\rho/\mu$ and the equivalent sand roughness of the wall $k$ with Churchill's equation (Churchill, 1977), which is equivalent to the well-known Moody diagram:

$$f = 2\left[\left(\frac{8}{\mathrm{Re}}\right)^{12} + (A + B)^{-1.5}\right]^{1/12} \tag{1-6}$$

where

$$A = \left\{-2.457 \ln\left[\left(\frac{7}{\mathrm{Re}}\right)^{0.9} + \frac{0.27k}{D}\right]\right\}^{16}$$

and

$$B = \left(\frac{37530}{\mathrm{Re}}\right)^{16}$$

## 1.2 TURBULENT PIPE FLOW

With its rapid mixing of neighboring fluid elements, turbulent flow consumes a great deal more energy than the simple gliding of fluid layers in laminar flow. This increased energy consumption accompanies an increase in the wall shear stress $\tau_w$ and in the other stresses within the flow. There are numerous turbulence models and new theories and computational techniques are still being developed (Lumley, 1990). In this section we summarize a few simple formulas that are used in subsequent sections of this book.

For the simplest flow situation, where the $x$-wise velocity varies only with $y$, the stress $\tau_{yx}$ in turbulent flow is expressed in terms of the velocity fluctuations associated with the turbulence, $v_x'$ and $v_y'$, by Equation 1–7.

$$\tau_{yx} = \rho\overline{v_x'v_y'} - \mu\frac{dv_x}{dy} \tag{1-7}$$

where $y$ is measured from the axis of symmetry of the flow. The two terms on the right-hand side of Equation 1–7 represent the inertial or turbulent Reynolds stress and the viscous shear contributions to the total stress. The bar superscript denotes a time average and the sign convention for stresses is the same as that used by Bird et al. (1960).

Strictly speaking, $v_x$ in Equation 1–7 should have a bar superscript too, but this was omitted in Equation 1–2. The term $\rho\overline{v_x'v_y'}$ is dominant except in the thin viscous sublayer at the wall.

The fact that a momentum equation can be written either for instantaneous values or time-averaged values of velocities, with alterations in the meaning of the stresses, is potentially confusing. It is usually necessary to inspect a derivation

carefully to see which approach is being used. We shall see that the same considerations apply to fluid–particle systems.

In principle, one integrates Equation 1–7 in the direction normal to the wall to find $V$ in terms of $\Delta P$ if one can relate $\rho\overline{v_x'v_y'}$ or, for pipes, $\rho\overline{v_x'v_r'}$, to the gradient of $v_x$. The integration gives $v_x$ as a function of $r$. This velocity distribution should reproduce the experimentally determined Law of the Wall. For smooth walls, the experimental data for homogeneous fluids fit the equation

$$\frac{v_x}{u_*} = \left(\frac{1}{\kappa}\right) \ln\left(\frac{u_*(0.5D - r)\rho}{\mu}\right) + A \tag{1–8}$$

where $u_*$ is the friction velocity $(\tau_w/\rho)^{0.5}$. Approximate values of $\kappa$ and $A$ are 0.4 and 5.75. An expression for both smooth and rough pipes (Roco, 1980) is

$$\frac{v_x}{u_*} = 8.48 - 5.75 \log_{10}\left(\frac{k}{0.5D - r} + \frac{3.3\mu}{\rho u_*(0.5D - r)}\right) \tag{1–9}$$

An eddy kinematic viscosity $\nu_t$ is used in the intermediate steps of the prediction of $v_x$ as a function of position. In its simplest form it is defined by Equation 1–10

$$\nu_t \frac{dv_x}{dy} = -\overline{v_x'v_y'} \tag{1–10}$$

$\nu_t$ is a function of position as well as $u_*$. A useful empirical expression for $\nu_t$ in fully turbulent pipe flow (Roco and Frasineanu, 1977) is

$$\nu_t = 0.146\, u_*\left(\frac{D}{2}\right)\left[1 - \left(\frac{2r}{D}\right)^2\right]\left[\left(\frac{2r}{D}\right)^2 + 0.54\right] \tag{1–11}$$

## 1.3 PARTICLE SIZE DISTRIBUTIONS

The size, density, shape, and surface texture of particles affect their behavior in a fluid–particle mixture. The size can be defined in a variety of ways, which depend upon the method used to make the measurements. These include:

1. an equivalent diameter, determined from particle volume, $V_p$, or surface, $S_p$. There are at least two possibilities:

$$d_V = \left(\frac{6V_p}{\pi}\right)^{1/3} \tag{1–12a}$$

$$d_S = \left(\frac{S_p}{\pi}\right)^{1/2} \tag{1–12b}$$

2. an equivalent diameter, determined from the settling velocity of a particle and a drag force relationship known to apply to spheres. This method is used frequently for very fine particles.
3. the sieve size, determined by the width of the minimum square aperture through which the particle will pass. This is the method that is used most often for coarse particles.

Since a mixture of sizes is invariably present, a size distribution curve should always be used to specify a mixture. Although log probability coordinates are sometimes used to detect bimodal distributions, the simple cumulative distributions shown in Figure 1–3 are usually sufficient to display measurements. If it is desirable to describe the size distribution quantitatively, several possible distributions are available (Allen, 1981). The simplest of these distributions are summarized in Table 1–1 as values of the cumulative fraction $P_s$ finer than screen size $d$. The parameters are $d_{50}$ (median size) and $m$ (dimensionless parameter) or the standard deviation $\sigma$. Frequently, more than one distribution appears to fit a given set of measurements fairly well.

Figure 1–3 shows some typical size distributions (solid lines) for industrial slurries and (dashed lines) Rosin–Rammler distributions, plotted as percentages coarser than size $d$. A Rosin–Rammler distribution with $m < 1$ can be considered broad, whereas one with $m > 2$ is comparatively narrow.

The particle shape and size is described more completely using image analysis (Beddow et al., 1984). This approach requires a high-resolution optical system and a computer.

Table 1–1. Two-Parameter Particle Size Distributions (Data from Allen, 1981)

| *Distribution* | $P_s = f(d)$ |
|---|---|
| Rosin–Rammler | $1 - \exp\left[-\ln 2\left(\frac{d}{d_{50}}\right)^m\right]$ |
| Gates–Gaudin–Schumann | $0.5\left(\frac{d}{d_{50}}\right)^m$ |
| Gaudin–Meloy | $1-\left[1-\left(\frac{d}{d_{50}}\right)\left(1-\sqrt[m]{0.5}\right)\right]^m$ |
| Log normal | $\left(\frac{1}{\sqrt{2\pi}}\right)\int_{-\infty}^{x}\exp\left(-\frac{t^2}{2}\right)dt$ where $x = \frac{\ln(d/d_{50})}{\ln \sigma}$ |

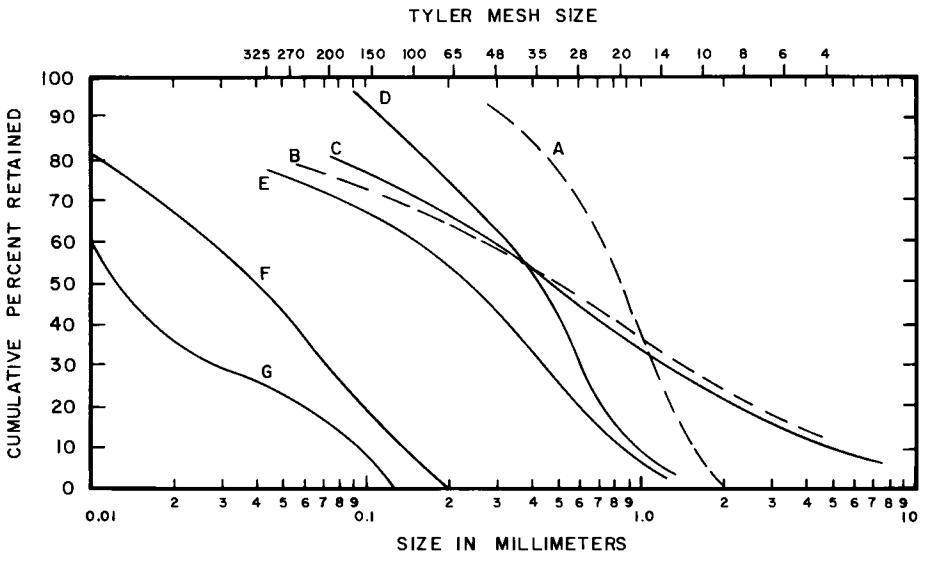


**Figure 1–3.** Some typical particle size distributions: A: Rosin–Rammler, $m = 2$; B: Rosin–Rammler, $m = 0.5$; C: −50 mm washed coal; D: potash (KCl) mill slurry; E: "long distance pipeline" coal slurry; F: boiler feed coal slurry; G: copper ore flotation cell underflow.

## 1.4 PACKING OF SOLID PARTICLES IN CONTAINERS

For uniform spheres, six regular arrangements are possible. The simplest of these are the *stacked* and the *close-packed* patterns. These are illustrated schematically in Figure 1–4 which shows the location of the particle centers in successive layers. The volume fractions of solids in the basic repeating units of these patterns are 0.5236 (stacked) and 0.7406 (close-packed rhombohedral). Other packing arrangements give concentrations between these limits. Random packing of large (negligible surface forces) spheres gives concentrations ranging between 0.59 (loose) and 0.64 (close) in the absence of wall effects. Smooth isometric particles, such as sand grains, give similar concentrations if the particle size distribution is narrow (Rosin–Rammler $m > 2$ or thereabouts).

Wall effects are important since the center of a basic packing unit cannot lie within $d/2$ of a wall and the volume fraction of solids at the tip of a sphere in contact with a wall approaches zero. This produces a lower volume fraction of the solid phase (higher local voidage) in the nearest layers as shown in Figure 1–5. As the ratio of particle diameter to container diameter increases, this effect causes the mean solid concentrations for randomly packed spheres to fall below the values quoted above.

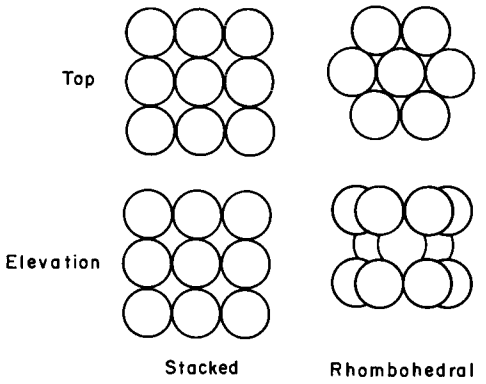


Figure 1–4. Two particle packing arrangements.

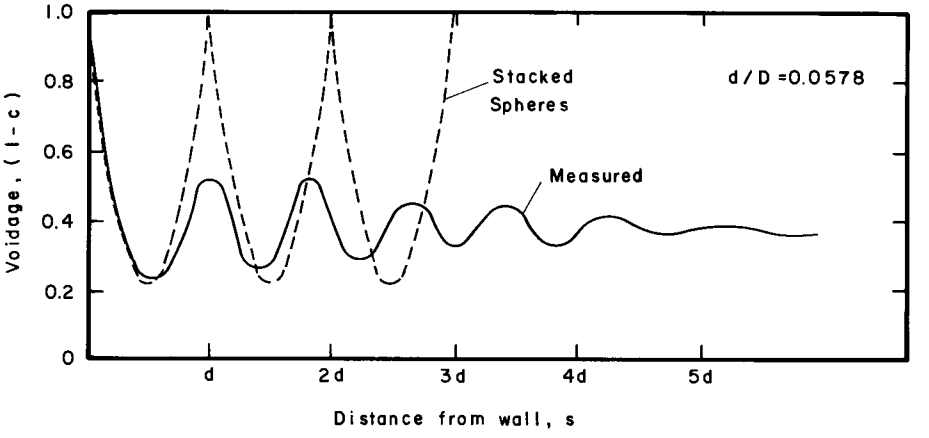


Figure 1–5. Voidage ($1 - c$) as a function of distance from the pipe wall. (Data from Ridgeway and Tarbuck, 1968.)

The *sphericity* of a particle is defined as the surface area of a sphere divided by the surface area of a particle of the same volume. As the sphericity decreases below its limiting value of unity, the concentration of packed beds of these particles also decreases. However, the concentrations differ less between the loose-packed and the close-packed conditions. Factors that increase the forces acting between particles, such as increased surface roughness or the presence of moisture to form bridges, favor the formation of voids of low concentration and cause the mean concentration of a packed bed to fall below the limits quoted earlier.

If a significant range of particle sizes is present, the concentration in a randomly packed bed can increase considerably. For example, a binary mixture of particles can contain more than 80% solids by volume if there is a very large difference in particle sizes. This is seen easily by considering a mixture of total volume equal to unity, in which the volume occupied by the larger particles is $c_2$.

Since there is a great difference in sizes, the smaller particles can be assumed to be uniformly distributed in the spaces between the large ones so that the volume occupied by the smaller particles is $(1 - c_2)c_1$, where $c_1$ is volume fraction of a fine particle in the space it occupies. The total volume of solids in this limiting case is then $c_2 + (1 - c_2)c_1$. With $c_2 = c_1 = 0.6$, this gives a total volumetric concentration of 0.84. High volumetric concentrations of mixtures with broad size distributions were considered by Asszonyi et al. (1972).

With sets of particles and diameters chosen to fill the interstitial spaces as fully as possible, even higher concentrations will be achieved. With spheres in an ordered arrangement, one obtains $c = 0.961$ using the so-called Horsfield packing.

## 1.5 FORCES ACTING ON A SINGLE PARTICLE IN A DILUTE SUSPENSION

A single particle moves in a fluid under the influence of the particle inertial force $\mathbf{F}_i$, the body force $\mathbf{F}_b$, and the net surface force $\mathbf{F}_f$.

$$\mathbf{F}_i + \mathbf{F}_b + \mathbf{F}_f = 0 \tag{1-13}$$

$\mathbf{F}_b$ is the resultant of a number of effects including fluid drag $\mathbf{F}_D$, fluid lift force $\mathbf{F}_L$, fluid inertia (added mass $\mathbf{F}_{am}$ and Basset history force $\mathbf{F}_{Bh}$), and the Brownian diffusion effect. The body force is caused by an external field (gravitational, electrostatic, or magnetic). The surface and inertial forces are relatively well understood for single particles but, as we shall see in subsequent chapters, at higher concentrations it is often necessary to estimate their magnitudes from the results of idealized calculations or experiments.

The motion of a single small particle in a turbulent fluid is described by the Basset–Boussinesq–Oseen equation (BBO equation) as explained, for example, by Wallis (1969) or Hinze (1975). In this context, "small" implies particle dimensions much smaller than the characteristic dimension of a turbulent eddy. However, to solve the equation, a description of the turbulent fluid motion is required and this is still a subject of research.

We shall see in subsequent chapters that the expressions for forces acting on particles in dilute systems are particularly useful in constructing dimensionless groups with which to characterize slurries and their flows.

## 1.6 DRAG FORCE ON IMMERSED OBJECTS

If $v$ is the velocity of a fluid relative to a particle of projected cross-sectional area $A_p$, the drag force in the direction of $v_r$ is calculated from an expression which defines the drag coefficient $C_D$.

$$\mathbf{F}_D = 0.5 C_D A_p \rho_L \mathbf{v}_r |v_r| \tag{1-14}$$

Equations 1–14 and 1–5 show the resemblance of $C_D$ to the friction factor $f$. $C_D$ depends on the shape and the Reynolds number $d|v_r|\rho_L/\mu$, where $d$ is a characteristic dimension of the particle and $\rho_L$ is the liquid density. $C_D$ also depends on the particle surface roughness, the degree of turbulence in the fluid, and the acceleration of the fluid relative to the particle. For steady flow past spheres, the relationship is given by Equation 1–15.

$$\begin{aligned} C_D &= \frac{24}{\mathrm{Re}_p} && \text{for } \mathrm{Re}_p = d|v_r|\rho_L/\mu < 0.2 \\ C_D &= \frac{24}{\mathrm{Re}_p}(1 + 0.15\ \mathrm{Re}_p^{0.687}) && \text{for } 0.2 < \mathrm{Re}_p < 1000 \\ C_D &= 0.44 && \text{for } 1000 < \mathrm{Re}_p < 3 \times 10^5 \end{aligned} \tag{1–15}$$

A single equation alternative expression for $C_D$ is

$$C_D = \frac{24}{\mathrm{Re}_p} + \frac{3.5}{\mathrm{Re}_p^{0.3}} + 0.23\ k \log_{10}\left(\frac{\mathrm{Re}_p}{1500}\right) \tag{1–16}$$

for $\mathrm{Re}_p < 7 \times 10^4$, $k$ is 0 for $\mathrm{Re}_p < 1500$ and 1 otherwise.

One of the simplest methods for determining $C_D$ is to measure the terminal falling velocity of a single particle in a large container. When the particle density is greater than that of the fluid, the immersed weight of the particle acts downward and $V$ is an upward velocity numerically equal to the terminal velocity because the fluid velocity is negligible. Since the forces must balance, we have

$$(\rho_s - \rho_L)g\left(\frac{\pi d^3}{6}\right) = 0.5C_D\left(\frac{\pi d^2}{4}\right)\rho_L\, v_r|v_r|$$

Using the symbol $V_\infty$ for the value of $v_r$ in this situation (infinite dilution), we have the important expression

$$V_\infty = \left(\frac{4gd(S_s - 1)}{3C_D}\right)^{0.5} \tag{1–17}$$

When settling takes place in a tube, the container boundary increases the drag force by retarding the fluid in its upward motion. If $V_s$ is the measured settling velocity in a container of diameter $D$, the infinite dilution velocity $V_\infty$ is given approximately by Francis's correction ($\mathrm{Re}_p < 1$):

$$V_\infty = V_s\left[\left(1 - \frac{0.475d}{D}\right) \Big/ \left(1 - \frac{d}{D}\right)\right]^4 \tag{1–18}$$

Corrections for other conditions are given by Clift, Grace, and Weber (1978). These corrections are important when $C_D$ is determined from measurements of $V_\infty$.

For irregular particles, settling is much more complicated because a measurement will determine the drag force for a preferred orientation reflecting the balance of moments of the forces exerted by the fluid on the surface of the particle. The terminal velocity is no longer a function of a single characteristic dimension of the particles but depends on shape and orientation.

For flowing slurries, settling is important because it influences the concentration distribution and because settling measurements are convenient techniques for particle characterization.

Heywood's volumetric shape factor (Clift et al., 1978) probably provides the most useful correlation for the effect of shape on the terminal velocity. The shape factor $k$ is defined in terms of the particle volume $V_p$ and the projected area diameter $d_A$:

$$k = \frac{V_p}{d_A^3} \tag{1-19}$$

where

$$d_A = \left(\frac{4A_p}{\pi}\right)^{0.5}$$

The particle shape can be characterized by other shape coefficients, such as the sphericity $\Psi$. If $S_p$ is the surface area of the particle, in terms of the diameters $d_V$ and $d_S$ defined in Equations 1–12a and 1–12b,

$$\Psi = \pi\left(\frac{6V_p}{\pi}\right)^{2/3} \Big/ S_p = \frac{d_V^2}{d_S^2} \tag{1-20}$$

Frequently, the particle shape is included in the equivalent particle diameter. For instance, the Stokes diameter is defined as

$$d_{\text{Stokes}} = \left(\frac{18\mu V_\infty}{(\rho_s - \rho_L)g}\right)^{0.5} \tag{1-21}$$

for $\text{Re}_p < 0.2$.

Of course, these methods of describing particle shapes must be related. For example, Pettyjohn and Christiansen (1948) found that, for isometric particles settling at very low Reynolds numbers,

$$\frac{d_{\text{Stokes}}^2}{d_V^2} = 0.842 \log_{10}\left(\frac{\Psi}{0.065}\right) \tag{1-22}$$

Although, in principle, the shape factor can be used as a correlating parameter to determine particle drag coefficients, the simplest way to determine particle settling velocities is to measure them.

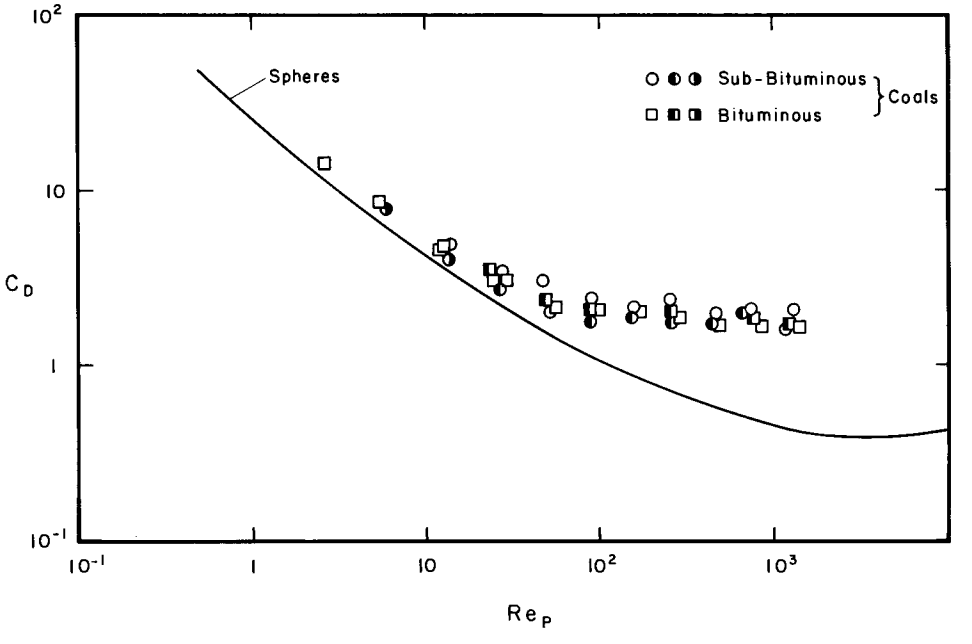


**Figure 1–6.** Particle drag coefficients for coals.

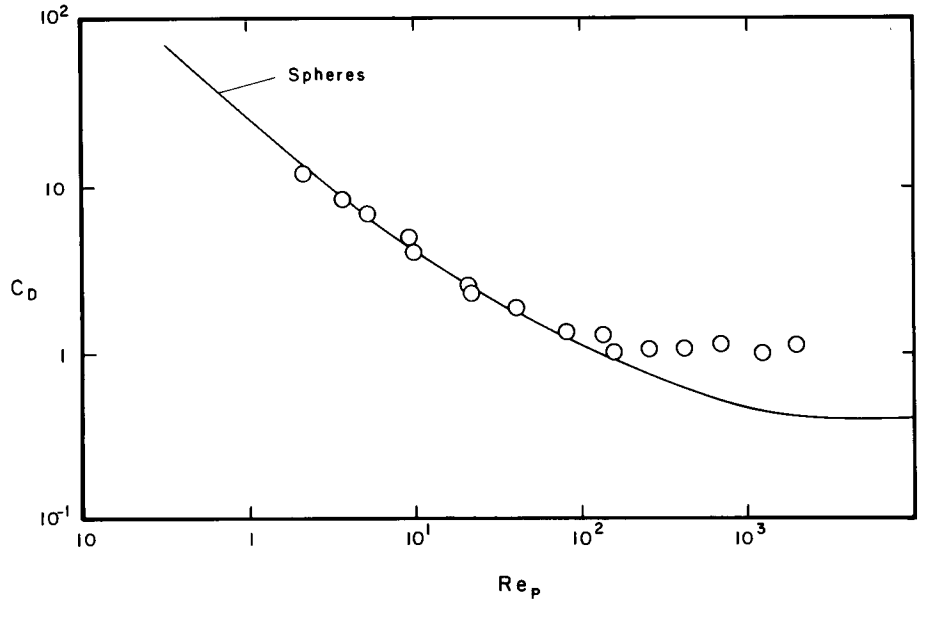


**Figure 1–7.** Particle drag coefficients for sands and gravels.

**Table 1–2.** Particle Drag Coefficients

| *Particle* | *Range* | $a_1$ | $b_1$ |
|---|---|---|---|
| Coal | Ar < 24 | 576 | −1 |
| | 24 < Ar < 4660 | 128 | −0.482 |
| | 4660 < Ar | 2.89 | −0.0334 |
| Sand | Ar < 24 | 576 | −1 |
| | 24 < Ar < 2760 | 80.9 | −0.475 |
| | 2760 < Ar < 46100 | 8.61 | −0.193 |
| | 46100 < Ar | 1.09 | 0 |

For high Reynolds numbers, ($10^3 < \mathrm{Re}_p < 10^5$), $C_D$ becomes independent of fluid viscosity so that empirical correlations for settling velocity can relate $V_\infty$ to particle size and the density ratio $S_s = \rho_s/\rho_L$. An empirical formula for large natural sand and gravel particles is

$$V_\infty = \left(\frac{8.925}{d}\right)\left\{\left[1 + 95(S_s - 1)\, d^3\right]^{0.5} - 1\right\} \tag{1–23}$$

where $V_\infty$ is expressed in mm/s and $d$ in mm.

In practice, $V_\infty$ should be measured if reliable values are required. Figures 1–6 and 1–7 show typical experimental results for coal, and sand and gravel particles. $C_D$ is correlated conveniently with the Archimedes number $C_D\mathrm{Re}_p^2 = 4d^3g(S_s - 1)\rho_L^2/3\mu_L^2 = \mathrm{Ar}$ that removes the necessity for iteration in calculating particle settling velocities.

Table 1–2 gives the coefficients of the piecewise fits of these results to equations of the form

$$C_D = a_1\left(C_D\mathrm{Re}_p^2\right)^{b_1} \tag{1–24}$$

These coefficients provide an indication of the importance of particle shape in settling measurements. The coal particles were fractured by mining and cleaning processes and had sharp edges and corners. The sand particles were rounded to some extent and had lower drag coefficients than the coals. $V_\infty$ values for the coarsest of the sands and gravels of Table 1–2 were about 20% higher than those predicted by Equation 1–23 and this difference reflects shape differences between particles from different sources.

Pairs and other clusters settle more quickly than single particles because the effective immersed weight of the aggregate (including any entrapped fluid) increases more rapidly with its volume than does the effective surface area. Such clusters form spontaneously in fluid–particle mixtures of low and moderate concentration. This complicates the tendency toward a reduced settling velocity which normally occurs as the concentration of the dispersed phase increases, and which is discussed in Chapter 2.

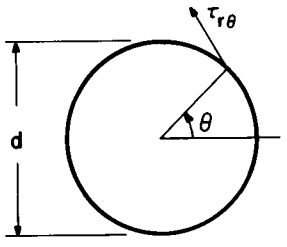


**Figure 1–8.** Effect of a fluid stress in supporting a particle.

For settling to occur in a fluid which has a yield stress $\tau_y$, the resisting stress in sheared fluid must be at least equal to $\tau_y$. (A definition of the yield stress can be found in Appendix 1.) If we assume the particle surface stress is everywhere equal to $\tau_y$, we can calculate the minimum particle diameter for which settling will occur. The vertical component of the shear force exerted on the surface is given in terms of the yield stress by the integral (see Figure 1–8)

$$0.5\pi d^2 \tau_y \int_{-\pi/2}^{\pi/2} \cos^2\theta \, d\theta$$

Since this force could balance the immersed weight of the sphere, we obtain Equation 1–25 for the diameter of the smallest particle which will settle.

$$d_{\min} = \frac{1.5\pi\tau_y}{(\rho_s - \rho_L)g} \tag{1–25}$$

Experiments appear to confirm that Equation 1–25 applies for particles immersed in stationary fluids with yield stresses. However, if motion of the particle relative to the fluid occurs, the critical size can be considerably different (Atapattu et al., 1988). The discrepancy is probably due to the fact that the surface shear stress need not be $\tau_y$ in the region of sheared fluid which forms at the surface of the particle (Beris et al., 1985).

When the fluid is non-Newtonian the drag coefficient will depend on all the rheological parameters of the fluid. For Bingham fluids, the drag coefficient is usually expressed in terms of the Reynolds number $\mathrm{Re}_p = dV_\infty \rho_L / \mu_p$ and the Bingham number $\mathrm{Bi} = \tau_y d / V_\infty \mu_p$. These two groups arise naturally if one defines a Reynolds number as the ratio of inertial forces, proportional to $\rho V_\infty^2$, to viscous forces that are proportional to $(\tau_y + K'\mu V_\infty / d)$, where $K'$ is a constant. Ansley and Smith (1967) evaluated the constant $K'$ to obtain the group $\mathrm{Re}_p/(1 + 7\pi\mathrm{Bi}/24)$ as an appropriate correlating parameter for drag coefficients. Alternatively, Dedegil (1986) suggested, in effect, that the denominator in the parameter could be taken as $(1 + \mathrm{Bi})$.

Hanks and Sen (1983) generalized the Ansley and Smith criterion to obtain the settling parameter $q$ for yield–power law fluids. The definitions of $\tau_y$, $n$, and $K$ are given in Appendix 1.